AIP Applied Physics Letters

Ring-based ultrasonic virtual point detector with applications to photoacoustic tomography

Xinmai Yang, Meng-Lin Li, and Lihong V. Wang

Citation: Applied Physics Letters **90**, 251103 (2007); doi: 10.1063/1.2749856
View online: http://dx.doi.org/10.1063/1.2749856
View Table of Contents: http://scitation.aip.org/content/aip/journal/apl/90/25?ver=pdfcov
Published by the AIP Publishing

Ring-based ultrasonic virtual point detector with applications to photoacoustic tomography

Xinmai Yang,[a] Meng-Lin Li, and Lihong V. Wang[b]
Optical Imaging Laboratory, Department of Biomedical Engineering, Washington University in St. Louis, One Brookings Drive, Campus Box 1097, Saint Louis, Missouri 63130

(Received 2 April 2007; accepted 24 May 2007; published online 19 June 2007)

An ultrasonic virtual point detector is constructed using the center of a ring transducer. The virtual point detector provides ideal omnidirectional detection free of any aperture effect. Compared with a real point detector, the virtual one has lower thermal noise and can be scanned with its center inside a physically inaccessible medium. When applied to photoacoustic tomography, the virtual point detector provides both high spatial resolution and high signal-to-noise ratio. It can also be potentially applied to other ultrasound-related technologies. © *2007 American Institute of Physics*. [DOI: 10.1063/1.2749856]

Photoacoustic tomography (PAT) has been shown to have great potentials in biomedical imaging.[1,2] One factor that limits the spatial resolution of PAT is the aperture size of the ultrasonic detector.[3–7] In practice, the aperture effect may be reduced by using a small point ultrasonic detector. However, because of large thermal noise, a small point ultrasonic detector has never been used in PAT.

Large size planar or line ultrasonic detectors have been studied previously.[8,9] We propose a ring-based virtual point detector and demonstrate its application in PAT. The virtual point detector provides PAT with the advantages of a real point detector, i.e., high and uniform spatial resolution throughout the field of view. At the same time, it produces much lower thermal noise than a real point detector. Our study is limited to two dimensions but can be extended to three dimensions.

In response to an impulse $\delta(t)$ point ultrasonic source within the ring, the pressure received by a ring-shaped ultrasonic detector, whose geometry is shown in Fig. 1(a), is given by

$$p_r(t) = \frac{1}{2\pi}\int_0^{2\pi} \frac{\delta(t - R(\theta)/c)}{R(\theta)} d\theta, \tag{1}$$

where t denotes time, θ denotes the polar angle of a point on the detector surface with respect to the center of the ring, c denotes the speed of sound in the medium, and $R(\theta)$ denotes the distance from the point source to the detector surface at θ. Within the arrival time t_1 and departure time t_2 of the ultrasonic signal, Eq. (1) leads to

$$p_r(t) = \frac{c}{\pi R_0 d_0} \frac{1}{\sin\,\theta(t)}, \quad t_1 \leqslant t \leqslant t_2, \tag{2}$$

where R_0 denotes the radius of the ring detector, d_0 denotes the distance from the point source to the ring center, $\theta(t)$ denotes the solution to $R(\theta)=ct$. If the detector can be characterized by a bandwidth-limited impulse response $h(t)$, the output of the detector becomes

$$Q(t) = p_r(t) \otimes h(t) = \int_{t_1}^{t_2} \frac{c}{\pi R_0 d_0} \frac{h(t-\tau)}{\sin\,\theta(\tau)} d\tau, \tag{3}$$

where $\otimes$ denotes convolution.

The function $p_r(t)$ is infinite at $\theta=0$ and $\theta=\pi$, slow varying in between, and 0 elsewhere. Approximately, it resembles a rectangular function except at the rising and falling edges. If a rectangular function is convolved with $h(t)$ and the width of the rectangular function is much greater than the width of $h(t)$, the derivative of the convolution result recovers $h(t)$ at both the rising and falling edges. Therefore, the derivative of $Q(t)$ approximately recovers $h(t)$.

We now use a realistic pulse $h(t)$ to examine the detected signal. We choose $h(t)=At^{-3}\cos(2\pi f_0 t)e^{-Kf_0 t}$,[10] where A is a constant and f_0 is the center frequency (6 MHz here). With $K=3.833$, this function gives a frequency bandwidth of 80%. The original pulse shape is shown in Fig. 2(a). The signal received by a ring detector is shown in Fig. 2(b) and its time derivative in Fig. 2(c). The correlation coefficient is 0.97 between the original pulse and the first pulse in Fig. 2(c) and −0.97 between the original pulse and the second pulse in Fig. 2(c). These results show that the original impulse response $h(t)$ is approximately recovered in Fig. 2(c).

The above conclusion suggests that we can approximately obtain the response of a real point detector from that of a ring detector of the same frequency bandwidth. A concept of virtual point detector thus can be proposed as follows. When a ring detector is used to detect signals from a point target, an arrival signal associated with t_1 and a departure signal associated with t_2 will be received. The arrival signal is due to the wave that propagates away from the ring center and reaches the ring through the shortest path. By contrast, the departure signal is due to the wave that propagates toward the ring center and reaches the ring through the longest path. Conceptually, both the arrival and departure signals can be considered to have propagated through the ring center although the arrival signal does not physically traverse the ring center. The ring center thus can be treated as a virtual point detector. The derivatives of both the arrival and departure signals closely recover the signals that would be received by a real point detector.

The following process is used to recover the response of a point detector:

[a]Electronic mail: xmyang@biomed.wustl.edu
[b]FAX: (314) 935-7448; electronic mail: lhwang@biomed.wustl.edu

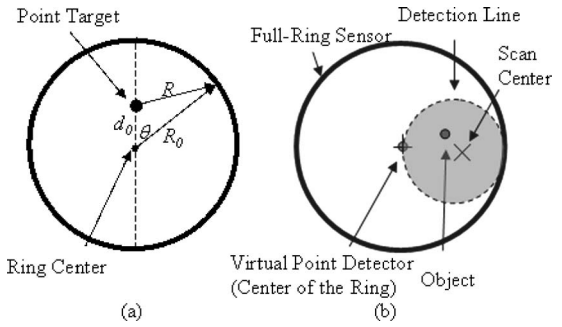

FIG. 1. Geometry of (a) the detection system and (b) 2D scanning when the virtual point detector is applied to PAT.

(1) Compute the acoustic propagation time t_c from the ring center to the ring.
(2) Separate the received signal into the arrival segment ($t \leqslant t_c$) and departure segment ($t \geqslant t_c$).
(3) Transform the time axis as $t_a = t_c - t$ for $t \leqslant t_c$ and $t_d = t - t_c$ for $t \geqslant t_c$, where t_a and t_d denote the current time axis for the arrival and departure signals, respectively.
(4) Take the time derivative of both signals, which produces two signals that are nearly identical to those that would be received by a real point detector.

After this process, either signal can be used to evaluate the spatial resolution and signal-to-noise ratio (SNR) of PAT.

A virtual point detector has lower thermal noise than a real one. The thermal-noise-induced rms voltage on an ultrasound detector can be written as $v_{\mathrm{rms}} = \sqrt{kT_0/C_T}$, where k is the Boltzmann constant, T_0 is the temperature of the sensor, and C_T is the capacitance of the detector. Because the capacitance is proportional to the square root of area of the detector, the voltage noise is inversely proportional to the area. Therefore, a real point detector has large thermal noise and hence cannot be used in practical PAT. Because a virtual point detector is constructed with a ring detector of a large surface area, it has much lower thermal noise than a real point detector.

We applied the virtual point detector to PAT and tested its performance with both simulation and experiment. A two-dimensional (2D) circular scanning detection geometry [Fig. 1(b)] and a simple back-projection algorithm[11] were employed to form an image. The scanning radius was 15 mm, and the scanning center was set as coordinates (0, 0). Pulse $h(t)$ shown in Fig. 2(a) was used as the received signals in the simulation. Both a real point detector and a finite-aperture (4 mm wide square) detector were tested for comparison with the virtual point detector. However, the scanning radius for the finite-aperture detector was set to 30 mm, instead of 15 mm, because 15 mm was too close to the finite aperture and resulted in poor resolution.

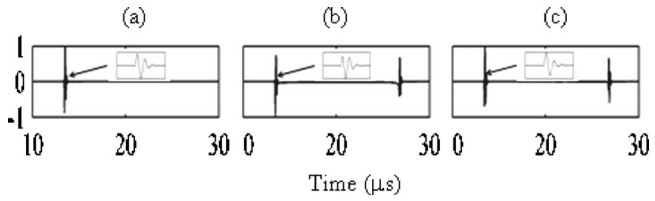

FIG. 2. Ultrasound pulse detected by a ring detector. (a) The original pulse shape, (b) the simulated signal detected by a ring detector, and (c) the time derivative of (b).

Simulated results for point targets are presented in Figs. 3(a)–3(c). In the forward problem, the detected signal was the sum of the three signals from the three point targets, each of which was computed as described above using Eq. (3). The envelopes of the received signals were used for image reconstruction. Figures 3(a)–3(c) show the images acquired with a virtual point detector with a ring diameter of 60 mm, a real point detector, and a finite-aperture detector, respectively. The virtual and real point detectors clearly produced equally high spatial resolution uniform over the entire imaged region. If the spatial resolution is defined as the half width of maximum amplitude, both the virtual and real point detectors yielded ~450 μm. The finite-aperture detector produced good spatial resolution near the scan center but poor tangential (y axis) resolution far from the center as expected[7] although the radial (x axis) resolution remained uniform. Note that the point target at $y = 10$ mm became a vertical line in Fig. 3(c), whereas the resolution along the x axis remained almost the same.

To obtain experimental results, we built a 60 mm diameter ring detector using 110-μm-thick polyvinylidene fluoride (PVDF) film. The detector had a center frequency around 6 MHz. We also built a 130-μm-wide square flat detector as a "real point detector" using PVDF film. This size was chosen to match the focal size, which we calculated by using the Rayleigh integral[12] of the finite-bandwidth ring detector. We further constructed a 4-mm-wide finite-aperture detector. The targets were black threads of 20 μm in diameter and placed perpendicularly to the scanning plane. A Q-switched Nd doped yttrium aluminum garnet laser (10 ns pulse width) (LS-2137/2, Symphotic TII Co. Camarillo, CA), operating at 532 nm with a pulse repetition rate of 10 Hz, was employed as the irradiation source. Samples were irradiated from the top and scans were performed on a horizontal plane. The photoacoustic signal was detected by the ultra-

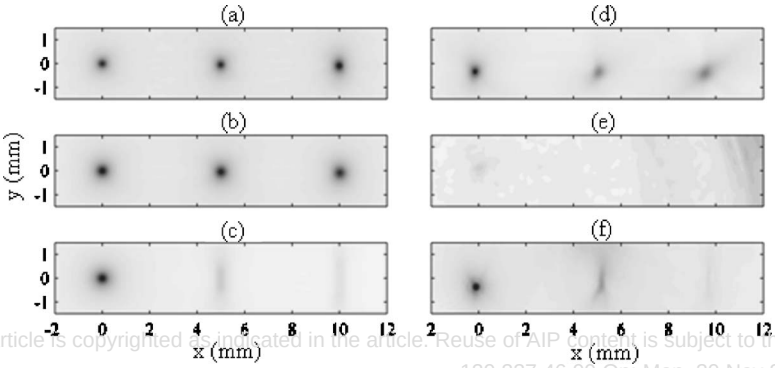

FIG. 3. Simulated images of point targets acquired using (a) a virtual detector, (b) a point detector, and (c) a finite-aperture detector. Experimental images of point targets acquired using (d) a virtual detector, (e) a point detector, and (f) a finite-aperture detector.

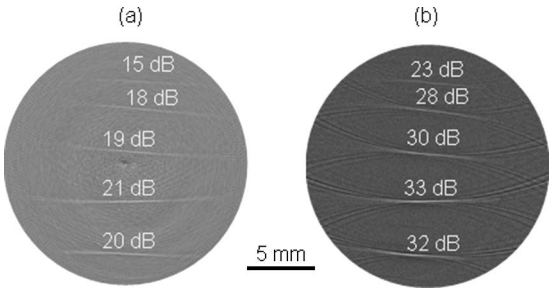

FIG. 4. Experimental images of line targets acquired using (a) a virtual detector and (b) a finite-aperture detector. Values of SNRs were evaluated in the middle of the lines.

sound detectors and amplified by a 50 dB amplifier (5072 PR, Panametrics, Waltham, MA). Next, the signal was directed to a digital oscilloscope (TDS5054, Tektronix, Beaverton, OR) and collected by a personal computer.

Experimental results for point targets are shown in Figs. 3(d)–3(f). For convenience, we refer to the point target near the scan center as target I, the one next to target I as target II, and the last point target as target III. As shown in Fig. 3(d), the virtual point detector produced constant spatial resolution of ~400 μm in the imaged area. This experimental result was similar to the simulated result shown in Fig. 3(a), except that point III was slightly defocused because the experimental scanning step size (1.5°/step) was coarser than the simulated one (1.0°/step). At the same time, the virtual point detector maintained relatively strong SNRs, which were 48, 44, and 39 dB for targets I, II, and III, respectively. By contrast, the image obtained with the real point detector had poor SNRs, and only target I could be identified with a 21 dB SNR. This experiment clearly showed that the virtual point detector had better SNR than the real point detector while maintaining good spatial resolution.

The images obtained with the finite-aperture detector had spatial resolution identical to that shown in the simulation. The SNRs obtained by the finite-aperture detector were 53, 39, and 25 dB for targets I, II, and III, respectively, which decreased quickly as the distance from the scan center to the target increased. By contrast, the SNRs yielded by the virtual point detector were more uniformly distributed.

Line targets, made of human hairs, were experimentally imaged. Figures 4(a) and 4(b) are acquired by the virtual point detector and the finite-aperture detector, respectively. As shown in Fig. 4(a), the virtual point detector produced uniform and good resolution along all lines throughout the field of view. In Fig. 4(b), the finite-aperture detector produced both good resolution and high SNR only in the middle part of the lines.

In the above images reconstructed from the virtual point detector, only the arrival segment of the signal was used. The SNR may be further improved if both the arrival and departure segments are used. Basically, the arrival and departure segments can be used separately to generate two images for the same object. The addition of the two images can improve the SNR of the final image because the signals from the two segments are correlated but the noises are uncorrelated.

In summary, we constructed an ultrasonic virtual point detector using the center of a ring transducer. The virtual point detector provides omnidirectional detection, which means that the detection is free of any aperture effect. Compared with a real point detector, the virtual point detector presented much lower thermal noise. Being the center of a physical ring, the virtual point detector can be scanned along a track inside a physically inaccessible medium to improve the resolution and SNR. We applied the virtual point detector to photoacoustic tomography and demonstrated that it yielded high resolution and strong uniformly distributed SNR. The virtual point detector can also be potentially used in other ultrasound-related technologies such as ultrasound tomography or pulse-echo-based ultrasonography.

This project was sponsored in part by National Institutes of Health under Grant Nos. R01 NS46214 and R01 EB000712.

[1]A. A. Oraevsky and L. V. Wang, Proc. SPIE **6086** (2006).
[2]M. Xu and L. V. Wang, Rev. Sci. Instrum. **77**, 041101 (2006).
[3]A. A. Oraevsky, R. O. Esenaliev, S. L. Jacques, S. Thomsen, and F. K. Tittel, Proc. SPIE **2389**, 198 (1995).
[4]A. A. Oraevsky, R. O. Esenaliev, S. L. Jacques, and F. K. Tittel, Proc. SPIE **2676**, 22 (1996).
[5]G. Ku and L. V. Wang, Med. Phys. **28**, 4 (2001).
[6]M. Xu, G. Ku, and L. V. Wang, Med. Phys. **28**, 1958 (2001).
[7]M. Xu and L. V. Wang, Phys. Rev. E **67**, 056605 (2003).
[8]M. Haltmeier, O. Scherzer, P. Burgholzer, and G. Paltauf, Inverse Probl. **20**, 1663 (2004).
[9]P. Burgholzer, C. Hofer, G. Paltauf, M. Haltmeier, and O. Scherzer, IEEE Trans. Ultrason. Ferroelectr. Freq. Control **52**, 1577 (2005).
[10]J. L. San Emeterio and L. G. Ullate, J. Acoust. Soc. Am. **92**, 651 (1992).
[11]M. H. Xu, Y. Xu, and L. H. V. Wang, IEEE Trans. Biomed. Eng. **50**, 1086 (2003).
[12]A. D. Pierce, *Acoustics-An Introduction to its Physical Principles and Applications* (Acoustical Society of America, New York, 1994), p. 214.